Respiratory and Rehabilitation Exercise Measurements Using Nanocomposite Wearable Sensors

XINYI YANG, TAYLOR PIERCE, DAVID STEN, ANDREW MARTINEZ, REGAN WAREHAM, CASSANDRA JAHN and KENNETH J. LOH

ABSTRACT

Diastasis recti abdominis (DRA), a common postpartum condition marked by the separation of the rectus abdominis muscles, can impair core stability, respiratory efficiency, and pelvic floor function. Despite the demonstrated clinical benefit of targeted exercise interventions, there is an urgent need for wearable technologies that could precisely assess rehabilitation progress and outcomes. This work presents a soft, low-profile, reusable, wearable sensor designed for high-resolution, real-time monitoring of abdominal mechanics during core-focused exercises. The skin-strain sensors were fabricated by sandwiching a multi-walled carbon nanotube thin film within two elastomer layers. Female participants with no history of childbirth were recruited to perform clinically relevant tasks, such as diaphragmatic breathing and various exercises. Wearable sensor skin-strain data, surface electromyography, and commercial respiration belt measurements were recorded for comparison. The results confirmed the system's ability to resolve task-specific variations in skin-strain while providing insights into muscle coordination and respiratory performance. The vision is to leverage these unique sensing streams to provide patients with real-time feedback while deriving data-driven, personalized rehabilitation strategies.

INTRODUCTION

Women, who give birth either via cesarean delivery or vaginal birth, are susceptible to various postpartum complications, including hemorrhage, infection,

Xinyi Yang[1], Taylor Pierce[1], David Sten[2], Andrew Martinez[3], Regan Wareham[2], Cassandra Jahn[2], and Kenneth J. Loh[1,*]

[1]Active, Responsive, Multifunctional, and Ordered-materials Research (ARMOR) Laboratory, University of California San Diego, La Jolla, CA 92093, U.S.A. *E-mail: kenloh@ucsd.edu

[2]S10 Fitness, 3810 Rosecrans St, San Diego, CA 92110, U.S.A.

[3]Built Well for Birth, 320 16th St, San Diego, CA 92101, U.S.A.

and prolonged recovery times [1, 2]. Among these, diastasis recti abdominis (DRA) is a prevalent condition characterized by the abnormal separation of the medial borders of the rectus abdominis muscles that exceeds 2 cm [3]. DRA often develops during late pregnancy and may persist into the postpartum period. It has been associated with impaired core stability, abdominal wall protrusion, pelvic floor dysfunction, and low-back pain. If left unmanaged, DRA may progress to more severe outcomes such as lumbopelvic instability, herniation, and visceral displacement [4]. Beyond physical impairments, changes in abdominal appearance can negatively impact self-image and psychological well-being, which contributes to body dissatisfaction and elevated emotional stress [5].

Targeted exercise interventions have shown clinical efficacy in restoring core function and mitigating DRA-related symptoms [6]. However, existing tools for monitoring rehabilitation progress are limited in scope. Most commercial wearable devices only track general metrics such as motion, heart rate, temperature, and blood pressure [7-9]. This limitation hinders the accurate evaluation of functional recovery and constrains the development of personalized rehabilitation strategies.

To address this unmet need, this work introduced a soft, low-profile, reusable wearable sensor for continuous, high-resolution monitoring of muscle engagement and respiratory effort during core-focused rehabilitation. The system couples a nanocomposite-based strain sensor with a custom wireless data acquisition (DAQ) node to achieve real-time skin-strain measurements associated with core activation and breathing dynamics [10]. The system was evaluated in women without a history of childbirth, performing clinically relevant tasks, including standard breathing and core bracing. Data from the wearable sensor, commercial respiration belt, and surface electromyography (sEMG) were analyzed to characterize abdominal mechanics [11].

EXPERIMENTAL DETAILS

Wearable Sensor Fabrication

The flexible, reusable, wearable skin-strain sensor was developed for direct skin contact while possessing high sensitivity to capture subtle physiological skin-strain changes during different movements. The sensors were fabricated by sandwiching a piezoresistive multi-walled carbon nanotube (MWCNT) thin film between two Ecoflex™ silicone elastomer layers (Figure 1). First, a base layer of Ecoflex™ was cast and cured on a glass substrate. Next, the active sensing layer was formed by sequentially drop-casting three layers of MWCNT ink to create a rectangular film, followed by thermal curing after each deposition step to ensure layer uniformity and adhesion. Electrodes were established by painting stretchable silver ink at both ends of the film before soldering single-strand wires. Finally, a top encapsulation layer of Ecoflex™ was applied and cured, forming a fully enclosed, stretchable device. The completed sensor was then peeled from the glass substrate and could be used as is.

Wireless DAQ Node Design

Data collection was accomplished using a custom-designed wireless DAQ board. This board was built around an ESP32-C3 (Espressif Systems), a 160 MHz RISC-V-

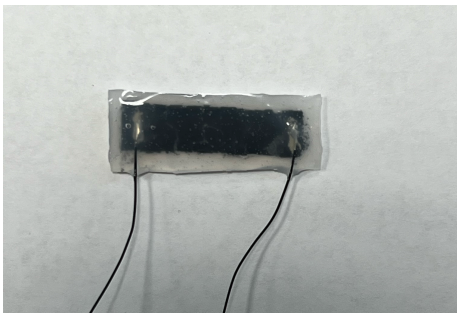

Figure 1. The wearable sensor with an MWCNT film sandwiched in elastomer layers

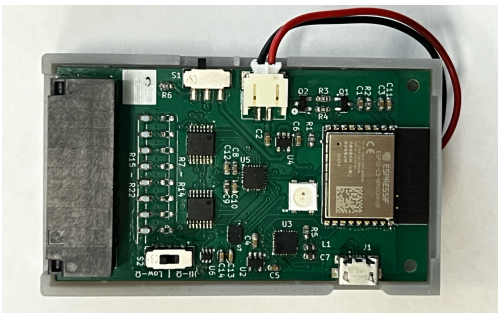

Figure 2. The top view of the wireless DAQ protected by a 3D-printed enclosure

based microcontroller with an integrated 2.4 GHz transceiver. The sensing streams were collected using a voltage divider network and the Analog Devices AD7689 analog-to-digital converter (ADC). This 16-bit successive approximation register (SAR) ADC includes a buffered reference voltage for low-noise and power supply isolation alongside a multiplexer and sequencer for simultaneous sampling across up to eight sensors. These components and supporting hardware (*i.e.*, power regulation, LED indicators, programming interface, and additional sensors) were assembled onto a custom printed circuit board (PCB) and housed in a 3D-printed enclosure (Figure 2). The final board was connected to a 3.7 V, 20,00 mAh lithium-ion polymer battery, with the DAQ consuming approximately 80 mA during active data collection.

The ADC was configured to sample at a high rate, with ~5 μs sampling time per channel, as it sequences across all eight channels. These sample points are packaged and transmitted over Wi-Fi for final data collection. The DAQ then holds for a short period before sampling again to achieve the desired net sampling rate of 200 Hz.

Electromechanical Characterization

Electromechanical tests were conducted using a Test Resources 100R load frame, which applied monotonic, uniaxial, tensile cyclic loads (*i.e.*, 20 cycles to a peak strain of 3.5%) to wearable sensor specimens. During testing, two-point probe electrical resistance was recorded using a Keysight 34465A digital multimeter operating at ~1.5 Hz. The load frame also recorded crosshead displacement (for calculating the applied strains) and applied load at a sampling rate of 20 Hz.

Human Participant Testing

The study protocol was approved by the University of California, San Diego Institutional Review Board (IRB) under Project No. 191806, and written informed consent was obtained from each participant. To enable targeted monitoring of the affected regions and to quantitatively assess participant performance during exercise tasks, wearable sensors were fabricated and strategically placed on the left and right external intercostal muscles, rectus abdominis, and rhomboid muscles (Figure 3). Each sensor was affixed onto the skin by applying 3M Tegaderm™ film over the sensor and skin area. The sensors were then connected to the wireless DAQ node. In parallel, sEMG data were collected at the same anatomical locations as the wearable sensors for comparative analysis of muscle activation. A commercial Venier

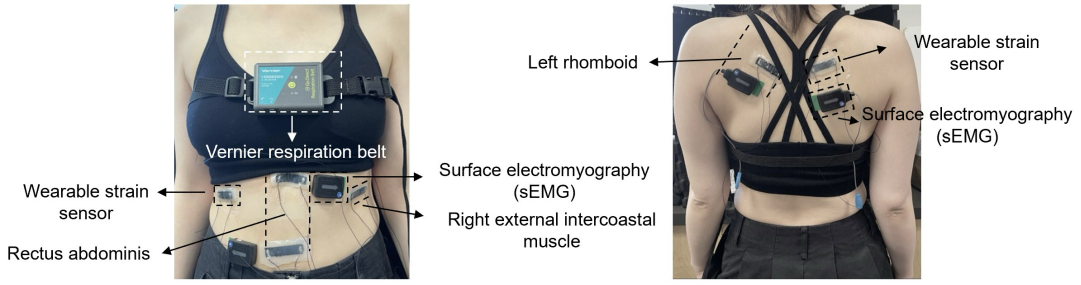

(a) (b)

Figure 3. Experimental setup on the subject (a) Anterior side and (b) Posterior side

respiration belt was also worn over the chest to serve as a reference for respiratory activity. The recorded signals were normalized to baseline values and processed using a basic outlier filter to remove corrupted data caused by wireless transmission artifacts.

Participants performed controlled activities to validate the wearable sensors. First, the subject completed three cycles of at-rest (normal) breathing. Second, three biceps curls were performed with weights while maintaining controlled breathing to evaluate essential muscle activation. Last, participants executed a standing crunch involving full-body extension, followed by flexion and a return to the upright posture. Distinct resistance peaks were anticipated across the various trials due to task-specific skin-strain profiles. To enhance consistency between tests and across participants, each individual was instructed to maintain (1) a fixed gaze point to stabilize visual reflexive tone, (2) a neutral head position to optimize vestibular alignment, and (3) a resting tongue position on the roof of the mouth during nasal breathing to create optimal neuromuscular activation and muscle recruitment efficiency. Foot placement was also standardized to ensure consistent proprioceptive feedback from the ground.

RESULTS AND DISCUSSION

Wearable Sensor Strain Sensing Properties

The strain sensing properties of the wearable sensor were characterized by tensile cylic load frame tests. Figure 4a presents a representative set of cyclic test results, where the normalized change in electrical resistance (ΔR_n) of the wearable sensor is overlaid with the applied strain pattern. Here, ΔR_n was calculated by:

$$\Delta R_n = (R_i - R_0)/R_0 \quad (1)$$

where R_i is the resistance of the sensor at any point in time, and R_0 is the initial unstrained resistance. Sensor measurements were normalized because each sensor had a slightly different R_0 as a result of experimental error from fabrication and mounting. The results confirmed the expected sensing behavior: electrical resistance increased with tensile strain and decreased with compression.

Furthermore, Figure 4b plots ΔR_n with respect to the applied strains for one particular loading cycle. It shows that the wearable sensor exhibits a strong bilinear sensitivity to applied strains. By fitting linear least-squares regression lines to the data in Figure 4b, the slope of the best-fit line was equivalent to the strain sensitivity,

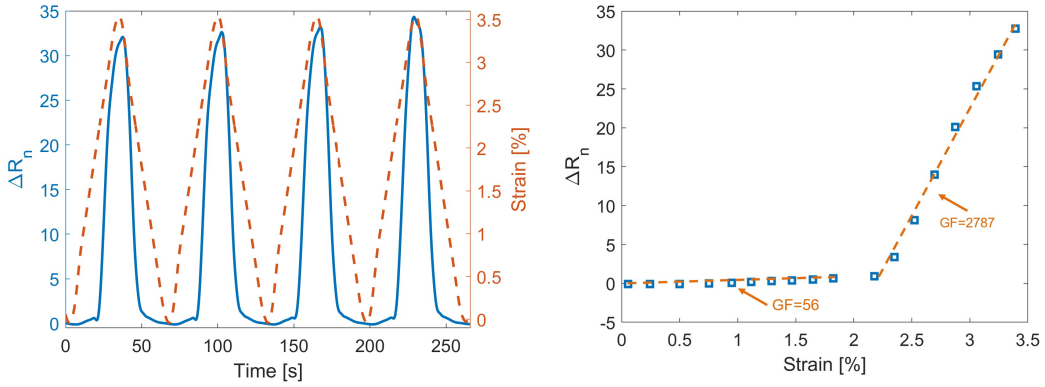

(a) (b)

Figure 4. Electromechanical testing of the wearable strain sensor: (a) normalized resistance overlaid with the applied strain pattern and (b) evaluation of sensor strain sensitivity

or gauge factor (GF), which was 56 when applied strains were below 2%. On the other hand, the sensor exhibited extremely high sensitivity when strains exceeded 2%.

Respiration Monitoring

The human participant tests began with normal breathing at a controlled pace. Figure 5 overlays the ΔR_n time histories collected from the set of six wearable sensors during three cycles of normal breathing. Distinct resistance peaks were observed from at least five wearable sensors, namely the sensors placed at both the left and right external intercostal, top rectus abdominis, and rhomboid muscles. These sensors were able to capture skin-strain associated with breathing because their placement aligned with regions of significant thoracoabdominal movement during respiration, allowing the skin-strain sensor to detect subtle surface deformations induced by muscle expansion and contraction. Notably, the sensor positioned over the top rectus abdominis displayed an opposite resistance trend relative to sensors placed at other anatomical sites.

The wearable sensor results were compared with force measurements from the Vernier respiration belt, with two of the five results overlaid in Figure 6. Even though

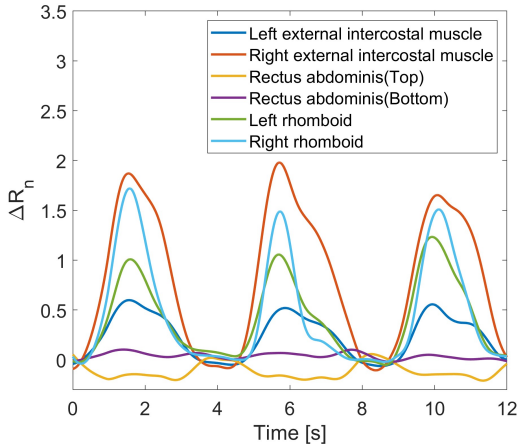

Figure 5. Skin-strain measurements during three cycles of normal breathing

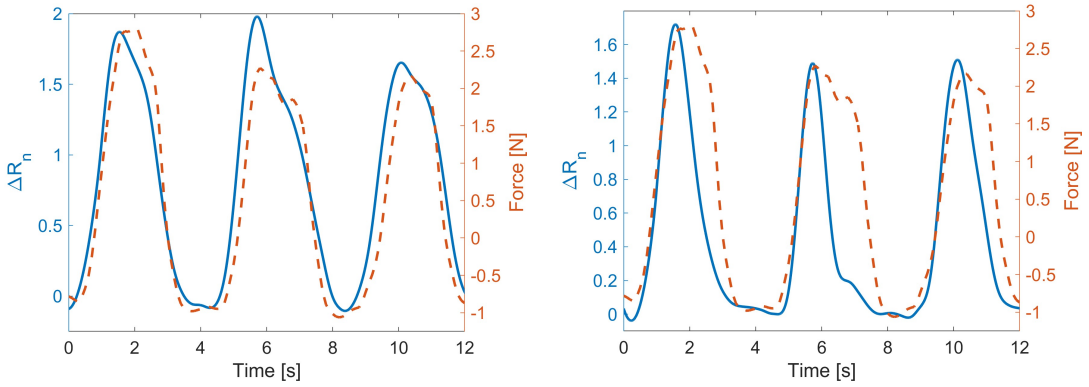

Figure 6. Skin-strain measurements (blue) were compared with sEMG readings (orange) at (a) the location of the right external intercostal muscle and (b) the right rhomboid

the two sensing systems measured different physical quantities, a strong agreement was observed. A dominant frequency of 0.25 Hz was identified from both the wearable sensor and Vernier respiration belt data, which equated to a respiration rate of 15 breaths per minute (bpm). These results successfully validated that the wearable skin-strain sensor mounted at these anatomical locations could accurately measure respiration rate. Unlike the Vernier respiration belt, which consisted of a rigid belt mounted across the chest and could slip over prolonged use, the proposed low-profile wearable sensor was secure, conformed to the skin, and was comfortable to wear.

Exercise Monitoring

The standing crunch was selected as a representative exercise to assess abdominal core engagement during recovery. Each subject completed three full-body crunches, each consisting of trunk flexion followed by a return to the upright position. A set of skin-strain measurements is plotted in Figure 7, where three distinct movement phases can be clearly identified. Each cycle of ΔR_n corresponded to skin-strain changes, as captured by the wearable sensor, during each full-body crunch. Notably, the sensors placed over the left and right rhomboid muscles exhibited larger resistance changes, indicating elevated back muscle activation during the exercise.

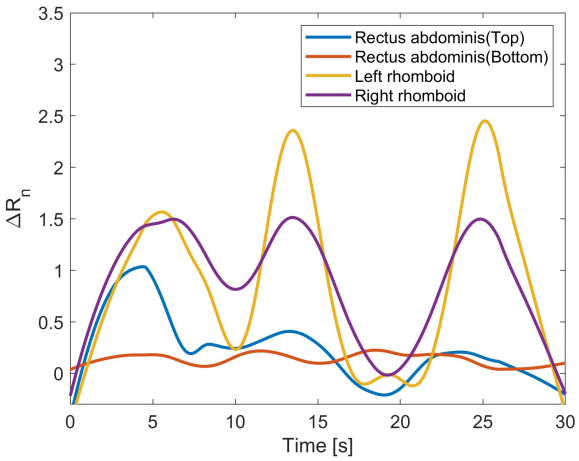

Figure 7. Skin-strain measurements during three cycles of standing crunches

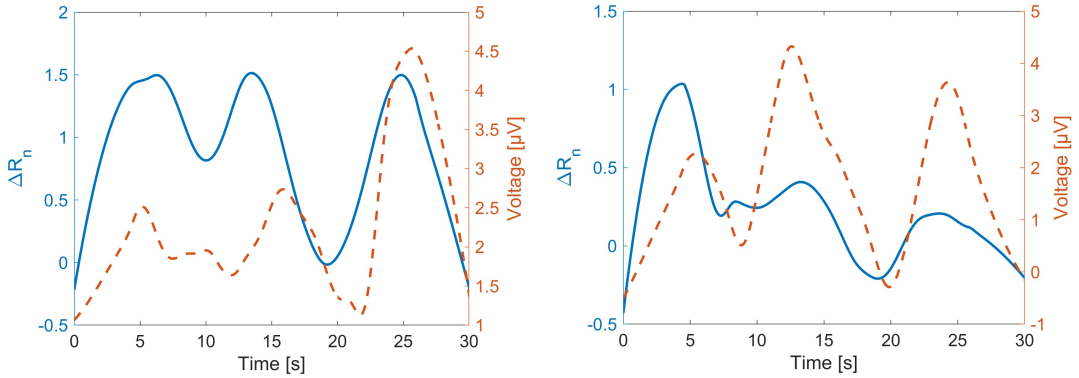

Figure 8. Skin-strain sensor data (blue) were compared with sEMG envelope results (orange) at the location of the (a) right rhomboid and (b) rectus abdominis (top)

The skin-strain data were further analyzed and compared with muscle activation measurements acquired from Delsys sEMG sensors, and two representative results are plotted in Figure 8. Figure 8 shows that the skin-strain ΔR_n and sEMG waveforms both exhibit three distinct cycles corresponding to the three full-body crunches. The normalized resistance change signal amplitude differences from cycle to cycle are expected since the wearable sensors measure skin-strain response, which is a combination of kinematics and potential skin-strains developed in response to greater muscle engagement [11]. Nevertheless, the sEMG data helped confirm that muscles in those specific areas were engaging to produce movement, which was also successfully captured by the wearable sensors.

CONCLUSIONS

This work evaluated the integration of wearable skin-strain sensors with a customized wireless sensing node, and the system was validated for capturing both respiratory and muscular engagement during controlled exercise movements. In particular, the wearable sensors successfully measured distinct electrical resistance waveforms during resting breathing and standing crunch exercises, underscoring their potential for monitoring rehabilitation activities. The long-term goal is to advance this system into a scalable, data-driven platform capable of enabling early detection of functional impairments and delivering personalized rehabilitation guidance. Future efforts will focus on extending its application to postpartum populations, including women recovering from cesarean delivery.

ACKNOWLEDGEMENTS

This research was partially supported by the U.S. Office of Naval Research (ONR) under grant no. N00014-23-1-2647, as well as gift funding from Leidos. This work benefited from the guidance of John Beck and Anders Olsson, whose expertise in respiratory biomechanics and breathing practices provided valuable insights throughout this study.

REFERENCES

1. Berghella, V., J. K. Baxter, and S. P. Chauhan. 2005. “Evidence-Based Surgery for Cesarean Delivery,” *Am. J. Obstet. Gynecol*., 193(5):1607–1617.
2. Cahill, A. G., N. Raghuraman, M. Gandhi, and A. J. Kaimal. 2024. “First and Second Stage Labor Management: ACOG Clinical Practice Guideline No. 8,” *Obstet. Gynecol*., 143(1):144–162.
3. Reinpold, W., F. Köckerling, R. Bittner, J. Conze, R. Fortelny, A. Koch, J. Kukleta, A. Kuthe, R. Lorenz, and B. Stechemesser. 2019. “Classification of Rectus Diastasis—A Proposal by the German Hernia Society (DHG) and the International Endohernia Society (IEHS),” *Front. Surg*., 6:1.
4. Kulli, H. D., and H. N. Gurses. 2022. “Relationship Between Inter-Recti Distance, Abdominal Muscle Endurance, Pelvic Floor Functions, Respiratory Muscle Strength, and Postural Control in Women With Diastasis Recti Abdominis,” *Eur. J. Obstet. Gynecol. Reprod. Biol*., 279:40–44.
5. Gopalan, P., M. L. Spada, N. Shenai, I. Brockman, M. Keil, S. Livingston, E. Moses-Kolko, N. Nichols, K. O’Toole, B. Quinn, and J. B. Glance. 2022. “Postpartum Depression—Identifying Risk and Access to Intervention,” *Curr. Psychiatry Rep*., 24(12):889–896.
7. Shaik, A., S. Khan, A. Shaik, K. K. Shaik, and M. S. Khan. 2024. “Advancements in Postpartum Rehabilitation: A Systematic Review,” *Cureus*, 16(8).
8. Pereira, K. A. J., S. Acharya, P. Bangera, and P. K. Rao. 2024. “Nurturhub: A Smart Maternal Health Monitoring Device for Post Partum Depression,” *Proc. IEEE Int. Conf. Distrib. Comput., VLSI, Electr. Circuits Robot. (DISCOVER)*, pp. 339–344.10. Matthews, J., I. Soltis, M. Villegas-Downs, T. A. Peters, A. M. Fink, J. Kim, L. Zhou, L. Romero, B. L. McFarlin, and W. H. Yeo. 2024. “Cloud-Integrated Smart Nanomembrane Wearables for Remote Wireless Continuous Health Monitoring of Postpartum Women,” *Adv. Sci*., 11(13):2307609.
9. Poudyal, A., A. Van Heerden, A. Hagaman, S. M. Maharjan, P. Byanjankar, P. Subba, and B. A. Kohrt. 2019. “Wearable Digital Sensors to Identify Risks of Postpartum Depression and Personalize Psychological Treatment for Adolescent Mothers: Protocol for a Mixed Methods Exploratory Study in Rural Nepal,” *JMIR Res. Protoc*., 8(9):e14734.
10. Lin, Y.-A., E. Noble, C.-H. Loh, and K. J. Loh. 2022. “Respiration Monitoring Using a Motion Tape Chest Band and Portable Wireless Sensing Node,” *J. Commer. Biotechnol*., 27(1):32–37.
11. Lin, Y.-A., Y. Mhaskar, A. Silder, P. H. Sessoms, J. J. Fraser, and K. J. Loh. 2022. “Muscle Engagement Monitoring Using Self-Adhesive Elastic Nanocomposite Fabrics,” *Sensors*, 22(18):6768.